Feasibility Study of a Sustainable, Low-Power Repeater for Repeater-Assisted MIMO Systems

Ybe Vandamme
ybe.vandamme@hotmail.com

Department of Electrical and Information Technology
Lund University

Supervisor: Sara Willhammar & Anders J Johansson

Examiner: Ove Edfors

July 24, 2025

Printed in Sweden
Tryckeriet i E-huset, Lund

Abstract

The rollout of 5G networks in rural or infrastructure-limited areas raises the question of how to power repeater systems in places where electrical grid access is limited or unavailable. This thesis investigates the feasibility of operating a 5G repeater entirely on solar power, with a focus on low energy consumption, compact integration, and realistic deployment scenarios.

An analog amplify-and-forward repeater architecture was examined for its potential to minimize power usage while maintaining acceptable performance. Commercially available components were analyzed to estimate power requirements, which were projected to be around 6.5 W. Various types of solar panels—including flexible CIGS and small crystalline silicon cells—were evaluated through hands-on measurements and literature review, with particular attention to their behavior under partial shading.

A charge controller with MPPT capability, based on the BQ25756 IC, was identified as a suitable option for energy harvesting under variable irradiance. Furthermore, solar energy availability across different European cities was analyzed to determine the viability of year-round solar-powered operation. The study concludes that fully autonomous solar operation appears feasible in southern locations, while hybrid or intermittent operation may be required in northern regions during the winter months.

This work provides a comprehensive exploration of the design considerations and environmental constraints involved in enabling off-grid, solar-powered 5G repeaters.

Declaration

I hereby affirm that this master thesis was composed by myself, that the work herein is my own, except where explicitly stated otherwise in the text. This work has not been submitted for any other degree or professional qualification except as specified; nor has it been published. Where other people's work has been used (either from a printed source, the internet, or any other source), it has been carefully acknowledged and referenced. During the preparation of this thesis, I have used ChatGPT to assist in the writing process to improve language, flow, and readability. After using this tool/service, I have reviewed and edited the content as needed, and I take full responsibility for the content of the whole thesis.

Acknowledgements

I would like to express my sincere gratitude to my supervisors, Sara Willhammar and Anders J. Johansson, for their invaluable guidance, support, and encouragement throughout this project. Their insights during our meetings, constructive feedback, and clear direction helped shape this thesis and made the process both educational and rewarding. I am especially thankful for their efforts in connecting me with experts in the field, which greatly enriched my understanding and allowed me to approach the topic from multiple perspectives. Their support not only helped me navigate technical challenges, but also provided the confidence to explore the broader implications of this work.

I would also like to extend my heartfelt thanks to my family and friends who visited me during my exchange. Your presence brought comfort, joy, and a much-needed boost of motivation during challenging times. Knowing that I had your support, even far from home, gave me the energy and encouragement to keep moving forward. Thank you for being there for me.

Popular Science Summary

Staying connected through 5G is becoming increasingly important—but what if you're in a location without easy access to electricity? In rural areas, construction sites, or even parts of a city with limited infrastructure, installing 5G repeaters to boost signal coverage becomes a real challenge. This thesis explores whether such devices can run entirely on solar power.

One key idea driving the project was to make the repeater easy to deploy anywhere in a city, without being visually disruptive. Early in the design process, the concept emerged to mount the device around existing traffic light poles or just poles to blend easily in the environment. This inspired a cylindrical form factor—wrapping solar cells around the pole itself rather than placing flat panels on top. The cylinder design offers several advantages: it preserves the visibility of traffic lights, blends more naturally into the urban landscape, and maximizes solar exposure throughout the day as sunlight shifts direction.

Instead of building a complete product, the research focused on energy needs and real-world feasibility. Components were carefully selected for low power consumption, and different types of solar panels were tested—both flexible and rigid—to assess performance in partial shading and variable light conditions. The results show that in sunny regions like southern Europe, a solar-powered repeater could run autonomously year-round. In less sunny places like Stockholm or Berlin, a hybrid setup combining solar and grid power may be more practical, especially during the winter months.

This study lays the groundwork for a new class of sustainable, low-impact 5G infrastructure—repeaters that can be installed quickly, operate off-grid, and fit seamlessly into the cityscape, all without needing a power outlet.

Table of Contents

List of Figures

List of Tables

Chapter 1

Introduction

1.1 Background and Motivation

Cellular communication technologies have continuously evolved to meet growing demands for faster, more reliable, and energy-efficient connectivity. Starting from basic voice services, cellular technology has expanded to high-bandwidth applications and diverse user demands. The introduction of 5G marked a significant leap, enabling not only higher data rates but also supporting Ultra-Reliable Low-Latency Communications (URLLC) and Massive Machine-Type Communication (mMTC). These advancements have made applications such as real-time remote operations, autonomous vehicles, and Internet of Things (IoT) deployments feasible.
To achieve these capabilities, developments were made that led to Multiple-Input Multiple-Output (MIMO) technologies. MIMO uses multiple antennas at both transmission and reception. This approach enhances capacity and improves reliability. Massive MIMO extends this concept by deploying hundreds or even thousands of antennas, further enhancing spectral efficiency, reducing interference, and increasing coverage through precise beamforming. However, the deployment of massive MIMO has some challenges, such as physical installation limitations, considerable energy consumption, and high operational costs. As wireless networks evolve toward the sixth generation (6G), the concept of Distributed MIMO, where antennas are spatially distributed yet coordinated, has emerged as a promising alternative. Distributed MIMO systems offer improved spatial diversity, better coverage, and reduced power consumption per unit.
Within this context, Repeater-Assisted massive MIMO (RA-MIMO) [1] systems have been proposed as an efficient solution. RA-MIMO uses compact, energy-efficient repeaters functioning as active scatterers, amplifying signals to provide improved coverage and capacity without requiring extensive base stations. The potential advantages of RA-MIMO systems include energy efficiency, simplified deployment, coverage enhancements, and suitability for challenging terrains.

1.2 Project Aims and Methodology

The primary aim of this master thesis is to explore the potential for designing a compact and energy-efficient repeater that could be powered by solar energy. The goal is not to deliver a final product, but to investigate whether such a system could be realistically built using commercially available components and within the constraints of power autonomy, cost, and installation simplicity.

To guide this investigation, the project followed a structured methodology:

- A literature review was conducted on existing repeater technologies, with a focus on analog amplify-and-forward architectures due to their simplicity and lower power usage. Both academic studies and commercial product specifications were analyzed to estimate typical energy demands
- The repeater concept proposed by Willhammar et al. served as a guiding framework for identifying system-level requirements such as low latency, channel reciprocity, etc.
- Multiple solar technologies were reviewed and tested—particularly flexible CIGS and small-scale crystalline silicon panels—to understand their performance under real-world constraints like partial shading and varying irradiance.
- Power consumption for each subsystem (LNA, PA, up/down converter, control unit, and modem) was estimated.
- Calculations were done to assess whether sufficient solar energy would be available throughout the year in different European cities.
- A Maximum Power Point Tracking (MPPT) charge controller based on the BQ25756 IC by Texas Instruments [2], was selected to manage energy harvesting efficiently across varying light conditions.

This thesis emphasizes the challenges, trade-offs, and constraints involved in the early-stage feasibility analysis of such a system. It highlights where current technologies fall short and where further innovation is required to make autonomous, sustainable 5G repeaters a practical reality.

Chapter 2
Repeater

The demand for 5G connectivity requires repeaters to extend signal coverage [3]. This chapter discusses the types of 5G repeaters and a design that is efficient and can work with renewable energy. Each functional block of the repeater is explained, and a detailed estimation of its average power consumption is presented.

2.1 Types of repeaters

Repeaters are devices that are used to receive, amplify, and retransmit wireless signals, thus expanding the coverage area of base stations. 5G networks can use various types of repeaters, which include the following:

- **Amplify-and-Forward (AF) Repeaters:** These repeaters amplify incoming signals and forward them without demodulation. They are simple, cost-effective, and introduce minimal latency.
- **Digital Repeaters:** These demodulate the received signal, process it (e.g., error correction) and retransmit. Although more flexible, they are power-intensive and complex. An example of such a repeater is presented in [4]
- **Network-Controlled Repeaters (NCR):** These are repeaters with remote control features, where parameters such as gain and operational state are managed by the base station. This allows energy-saving modes such as ON-OFF operation based on traffic demand.

In this project, an analog amplify-and-forward repeater with network control capability is selected to balance power efficiency and signal integrity.

2.2 Research about repeaters

First, various kinds of repeaters that are currently in use were investigated. This involved reading academic papers as well as exploring commercially available repeaters on the market. Various kinds of repeaters were investigated, ranging from small indoor models that simply extend the signal to larger outdoor units. These are listed in Table 2.1

Name Paper/website	Power Consumption	Information
Achieving Distributed MIMO Performance with Repeater-Assisted Cellular Massive MIMO [1]	10 W	
Airgain Lighthouse Micro smart repeater [4]	<40 W	Product on the market
Enabling On-Demand low-power mmWave repeaters via passive beamforming [5]	1 W	mmWave repeater
Increasing Cellular Network Energy efficiency for railway corridors [6]	28.4 W	Repeaters for trains
A novel portable repeater for 5G applications [7]	<3 W	Repeater for indoor use
Askey SCU2060 [8]	<100 W	Product on the market
WilsonPro Pro 70 Plus [9]	20 W	Product on the market
Surecall signal booster [10]	<25 W	Product on the market
Hocell 5G Cellular Signal Booster (HWSR-Pico Series) [11]	<10 W	Product on the market
Hocell 2T2R 5G Cellular Signal Booster [12]	<15 W	Product on the market
WilsonPro Network 257 [13]	34 W	Product on the market
WilsonPro Enterprise 1337 [14]	30 W	Product on the market

Table 2.1: Research, different repeaters

Their power consumption varied significantly. Therefore, it was necessary to carry out my own research by examining different components individually. For this, a meeting took place on 8 April 2025, with Lars Sundström from Ericsson, co-author of [1], who gave useful insight into the architecture of repeaters.

2.3 High level design

To better understand the power consumption of the AF-repeater, a detailed architectural overview is essential. Figure 2.1, adapted from the architecture presented in [1], illustrates this design. The chosen architecture—discussed and agreed upon with Lars Sundström, provides a comprehensive view of the total power consumption. Using a simplified architecture would likely lead to an inaccurate estimation. The parameters for the various components are based on the data from Willhammar et al [1].
The repeater consists of the following core blocks:

- Low Noise Amplifier (LNA)
- Up/down Converter
- Filter
- Power Amplifier (PA)
- Modem & Micro-controller

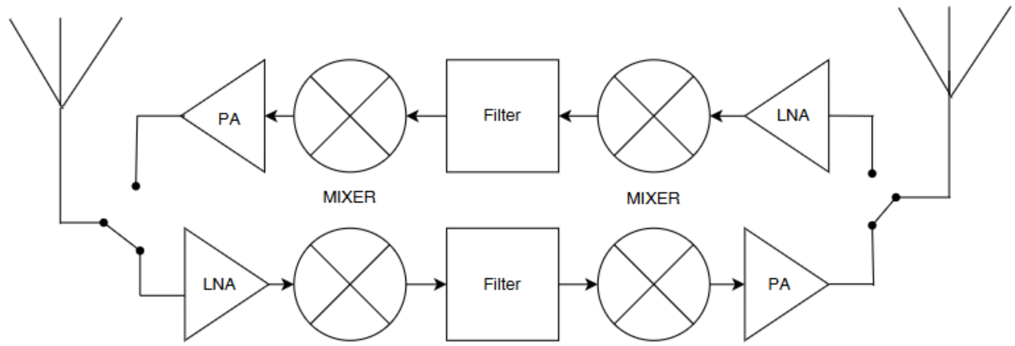

Figure 2.1: High-level design

2.3.1 Low Noise Amplifier (LNA)

The LNA amplifies weak incoming signals and adds minimal noise. A good LNA ensures that the repeater performs reliably, even at the edge of coverage areas. In Table 2.2, various commercially available components that meet the key criteria outlined in [1] are listed. These components were selected based on their compliance with performance requirements such as low noise figure and sufficient gain. To estimate a representative power consumption for such LNAs, an average was calculated from the listed components. This averaging approach provides a generalized power consumption value (0.4 W), reflecting a typical LNA used in similar applications rather than relying on a single, potentially non-representative device.

Company	**Component**	**Gain (dB)**	**NF (dB)**	**Power (mW)**	**Frequency (GHz)**
Qorvo [15]	QPL9057	22.8	0.54	250	0.6 – 4.2
	TQP3M9035	16.5	0.65	575	0.05 – 6
	QPL9058	18	0.6	275	0.5 – 6
	QPL9503	21.6	0.9	325	0.6 – 6
	QPL9547	19.3	0.3	325	0.1 – 6
	TQP3M9037	20	0.4	350	0.7 – 6
	SGL0622Z	28.5	1.5	34.7	0.005 – 4
	TQP3M9018	20.5	1.3	425	0.02 – 4
	TQP3M9019	22	1.3	625	0.02 – 4
	QPL7442	20	1.5	425	0.05 – 4
	SPF5043Z	12.9	0.8	230	0.05 – 4
	TQP3M9007	13	1.3	625	0.1 – 4
Analog Devices [16]	MAX2612	18.6	2	345	0.04 – 4
	MAX2613	18.6	2	256	0.04 – 4
	MAX2614	18.6	2	203	0.04 – 4
	ADL5523	21.5	0.8	300	0.4 – 4
	MAX2645	14.4	2.3	60	3.4 – 3.8
	HMC594	10	2.6	600	2 – 4

continued on next page

Company	Component	Gain (dB)	NF (dB)	Power (mW)	Frequency (GHz)
Skyworks [17]	SKY67189-369LF	18	0.69	260	0.4 – 6
	SKY67183-396LF	18.2	0.5	280	0.4 – 6
	SKY67181-396LF	22	0.58	240	2.3 – 6
	SKY67177-11	34	0.6	600	2.3 – 5
	SKY67180-306LF	31	0.8	625	1.5 – 3.8
	SKY67159-396LF	16.5	1.3	148.5	0.2 – 3.8
	SKY67153-396LF	16.5	0.7	400	0.7 – 3.8

Table 2.2: LNA components

2.3.2 Up/down converter

The RF signal is first down-converted to an intermediate frequency to simplify filtering and then up-converted back to the original 5G band. This frequency conversion can be implemented either across multiple modules or within a single integrated chip. To gain a more representative understanding of the power consumption associated with this process, various types of commercially available modules were examined, as shown in Table 2.3. These modules were selected based on their relevance to the intended application. Since some modules include only a single frequency converter while others integrate both up- and down-conversion stages, the power consumption values were normalized accordingly—doubling the power where only one stage was present to estimate full functionality. An average was then taken across these adjusted values to provide a global estimate of power consumption for this part of the repeater. This approach resulted in an estimated power consumption of approximately 1 W.

Company	Type	Power (W)
Arctic semiconductor [18]	IceWings	1.4
Analog Devices [16]	ADL5801	0.8
	AD9364	0.5
	AD9363	1.4
	LTC5562	0.1
	LTC5510	0.5
	AD8342	0.5
	ADL5801	0.7
Qorvo [15]	RFFC5071A	0.4
	RFFC5071A	0.5
	RFFC5072A	0.4

Table 2.3: Up/down converter components

2.3.3 Filters

The down-converted signal goes through band-pass filters to make sure only the right frequencies are amplified. These filters are generally passive and do not add to power use directly.

2.3.4 Power Amplifier (PA)

The power amplifier boosts the filtered and up-converted signal for transmission and is one of the main contributors to overall power consumption. To estimate a representative power usage for this component, several commercially available power amplifiers were examined based on the criteria defined in [1]. These examples, listed in Table 2.4, were selected to reflect realistic usage in a setup like the one under consideration. An average was then calculated from these components to obtain a more global estimate of the power consumption of a typical PA in this context. This approach resulted in an estimated consumption of approximately 2.2 W.

Company	**Component**	**Gain (dB)**	**Power (W)**	**Frequency (GHz)**	**Output Power (dB)**
Qorvo [15]	QPA9942	30.5	2.46	3.3 – 3.8	28
Analog Devices [16]	HMC409	31	3.075	3.4 – 3.6	30.5
	HMC327	21	1.25	3 – 4	21
Skyworks [17]	SKY66313-11	37	2	3.4 – 3.6	23 - 27
	SKY66318-11	35	2.2	3.3 – 3.6	32

Table 2.4: PA components

2.3.5 Control and communication

For remote control, a low-power modem (LTE Cat M1) and a microcontroller are included to handle synchronization and diagnostics. The modem options considered are listed in Table 2.5. To estimate the power consumption of this component, several existing LTE Cat M1 modems were reviewed, and an average was taken to obtain a representative value suitable for further system-level calculations. This resulted in an estimated modem power consumption of 0.8 W. For the microcontroller, a typical estimated power consumption of 1 W was used based on similar applications. Combined, these components contribute approximately 1.8 W to the total power budget.

Company	Type	Power Consumption (W)
Ublox [19]	SARA-R410M	0.7
Quectel [20]	BG77	0.8
	BG96	0.9
	BG95	0.7
Cinterion [21]	EMS31	0.9
Multitech [22]	DragonFly nano	0.8

Table 2.5: Modem components

2.4 Power Consumption

Table 2.6 shows the average estimated power consumption of the 5G repeater system, as detailed above, with a 20% margin added for inefficiencies.

Component	Power Consumption (W)
LNA	0.4
PA	2.2
µController	1
Transceiver	1
Modem	0.8
20% overhead	1
Total Consumption	≈ 6.5

Table 2.6: Total Power Consumption

This power usage helps determine the size and placement of the solar panel, which is discussed in the next chapters.

2.5 Summary

This chapter explores different types of 5G repeaters, focusing on amplify-and-forward (AF) repeaters due to their simplicity and low power consumption. It justifies the selection of an analog AF repeater with network control capability. The chapter presents a high-level system design composed of core components such as the Low Noise Amplifier (LNA), Up/Down Converter, Filter, Power Amplifier (PA), and a modem with microcontroller. It then estimates the power consumption of each block using commercially available components, resulting in a total average consumption of approximately 6.5W, including a 20% buffer for inefficiencies.

Chapter 3

Solar Panel

3.1 Solar Panel Technology Options

The design of a solar-powered 5G repeater started with the idea of mounting the system on existing infrastructure, such as a traffic light pole. This required the solar solution to be lightweight, compact, and ideally flexible, to allow for easier installation on curved surfaces. During the initial research phase, we met with Professor Magnus Borgström, on 5 March 2025, who strongly recommended exploring CIGS (Copper Indium Gallium Selenide) solar panels. He highlighted their flexibility, durability, and relatively high efficiency (15–22%). Professor Magnus Borgström also suggested looking into Midsummer AB, a Swedish company that produces CIGS panels designed for integration on roofs. Their solar panels have an efficiency around 11.7% [23]. Further exploration led to Miasolé, another supplier of high-efficiency flexible CIGS panels with an efficiency of 16.5% [24].

Following this direction, the system was designed around a CIGS panel. As the project progressed a meeting took place on 8 May 2025, with Professor Uwe Zimmermann, who provided critical feedback on this approach. He questioned the practical benefit of flexibility in this context and instead proposed a more modular solution. He suggested using small monocrystalline or polycrystalline panels (the ones found in toys and other little electronic applications) and connecting them in parallel. He explained that such configurations are less sensitive to shadow. This is because if solar cells are placed in series, the current depends on the solar cell with the least amount of sunlight.

3.2 Copper Indium Gallium Selenide (CIGS)

CIGS solar panels offer several advantages. They are flexible and thin. These attributes make them appealing for integration on surfaces such as poles or streetlamps. However, a number of drawbacks emerged during the design evaluation:

- Cost: CIGS panels are significantly more expensive than crystalline alternatives.
- Practical necessity: The assumed benefit of flexibility turned out to have limited practical value due to the impact of shading. This is because CIGS solar panels are often manufactured in fixed series-parallel configurations, where multiple cells are connected in series. In such setups, even partial shading of a single cell can significantly reduce the current flow of the entire string, leading to substantial performance losses. As a result, the flexibility of the

panel becomes less relevant when the system's energy yield is constrained by these shading effects.

3.3 Polycrystalline Solar Cells

Given the limitations of CIGS panels in terms of cost, availability, and questionable practical benefit in this context, the focus shifted to crystalline silicon solar cells. These include both monocrystalline and polycrystalline types, which are widely used in consumer electronics and small-scale applications due to their low cost, decent efficiency (15%) [25–30], and structural rigidity. To verify their suitability for this repeater system, a series of hands-on experiments were conducted using various panel sizes and configurations under different lighting conditions.

3.3.1 Tests

To evaluate the recommendation from Professor Zimmermann, we conducted experiments using two different types of solar panels: standard 1W cells and smaller 50×50 mm cells. The purpose was to understand how various configurations—series, parallel, and combinations—affect the panels' electrical behavior under different conditions.
A simple test setup with variable resistive loads was used to generate I-V (current-voltage) and P-V (power-voltage) curves. By connecting different resistors across the output terminals of each configuration, we created varying load conditions. For each resistor, we recorded the voltage across the panel and the corresponding current. From this data, I-V curves were plotted directly, while power values were calculated as $P = V \cdot I$, resulting in the corresponding P-V curves. This method allowed us to observe the impact of electrical configuration on system behavior. In particular, we examined how series connections increase overall voltage, while parallel connections enhance current. These experiments also helped identify the strengths and weaknesses of each setup—such as how shading impacts series configurations more significantly than parallel ones. The following configurations were tested:

- 50×50 mm 1 Cell
- 50×50 mm 2 Cells Parallel
- 50×50 mm 2 Cells Series
- 50×50 mm 2×2 Configuration
- 50×50 mm 3×3 Configuration
- 1W 1 Cell
- 1W 3 Cells Parallel
- 1W 3 Cells Series

1W Solar Cells

Figure 3.1 presents the I-V and P-V characteristics of various configurations using 1W solar cells. All measurements were conducted under natural sunlight, which introduces some variability due

to environmental factors such as passing clouds, temperature fluctuations, and slight differences in solar irradiance over time.
Subfigures (a) and (b) show the performance of a single 1W solar cell, serving as a reference for comparison. It is important to note that only one individual cell was measured to produce this reference data. Therefore, any comparisons with multi-cell configurations may reflect both cell-to-cell variation and external conditions during measurement.
Subfigures (c) and (d) illustrate a parallel configuration of three 1W cells. As expected, the current output is significantly higher than that of a single cell, while the voltage remains nearly the same. Interestingly, the current here is more than three times that of the single cell. This deviation may be attributed to several factors:

- **Cell Variations:** Each cell can have slightly different performance characteristics due to manufacturing tolerances. If the three cells used in the parallel setup had individually higher current capacities than the single cell measured earlier, this could explain the increased output.
- **Sunlight Conditions:** Since the measurements were taken outdoors, varying sunlight intensity—caused by cloud movement or shifting sun angle—can affect the output significantly. It's possible that the parallel configuration was measured under more favorable light conditions than the single cell.
- **Temperature Effects:** Solar cell performance is sensitive to temperature. As cell temperature increases, voltage typically decreases slightly, while current can increase slightly [31]. Thus, differences in panel temperature during measurement can also contribute to the observed behavior.

Subfigures (e) and (f) show a series configuration of three 1W cells. In this case, the voltage increases proportionally with the number of cells, as expected, while the current is theoretically limited to the current of the lowest-performing cell. Interestingly, the current is not exactly equal to that of the single cell across the entire voltage range. In fact, at lower voltages, the series configuration exhibits slightly higher current than the single cell. This can again be explained by the same factors:

- **Sunlight and Environmental Variation:** The series configuration may have been tested under stronger illumination than the single cell.
- **Cell Selection:** The three cells used in the series arrangement could have slightly better current performance compared to the single reference cell.
- **Temperature Effects:** Slight temperature differences between the two test moments may also explain variations in current.

These observations highlight the complexities of real-world solar cell testing and the importance of considering both environmental conditions and component variability when interpreting results.
Overall, these results reinforce the general behavior of parallel configurations offering higher current (with constant voltage), and series configurations providing increased voltage (with limited current). Understanding these trends is crucial for optimizing the electrical design of power systems in RA-MIMO repeaters or other low-power embedded applications.

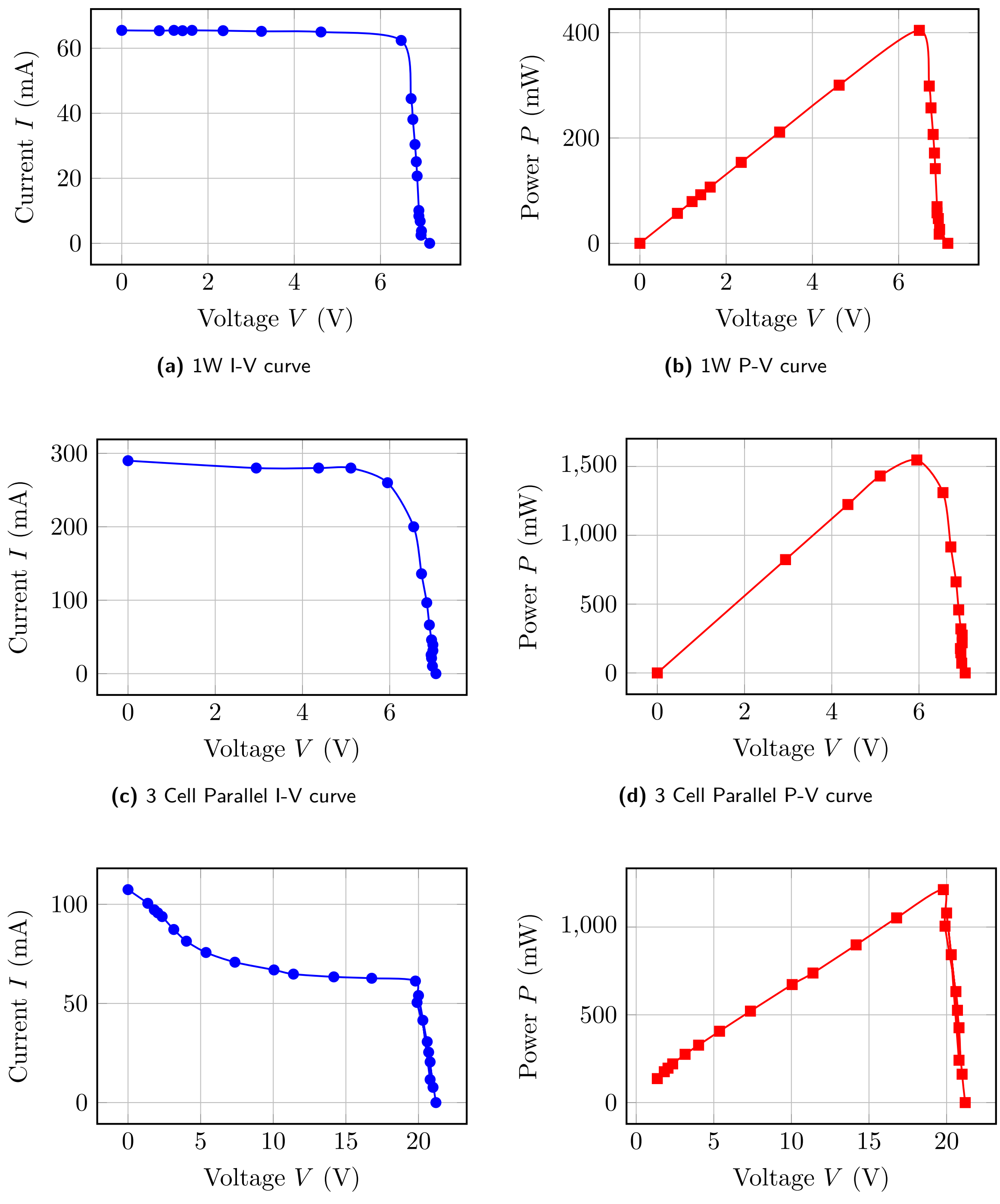

(a) 1W I-V curve

(b) 1W P-V curve

(c) 3 Cell Parallel I-V curve

(d) 3 Cell Parallel P-V curve

(e) 3 Cell Serie I-V curve

(f) 3 Cell Serie P-V curve

Figure 3.1: Comparison 1W solar cell

50×50 mm Solar Cells

Figure 3.2 shows the I-V and P-V curves for different configurations of small 50×50 mm polycrystalline solar cells.
Subfigures (a) and (b) illustrate the baseline performance of a single cell. Subfigures (c) and (d) present two cells in parallel, where the current increases while voltage remains nearly unchanged. Subfigures (e) and (f) show a series configuration of two cells, resulting in higher voltage output while maintaining the same current.
More complex arrangements are shown in subfigures (g) and (h) for a 2×2 matrix (two series-connected pairs connected in parallel), and subfigures (i) and (j) for a 3×3 configuration (three rows of three series-connected cells connected in parallel). The 3×3 setup yields a noticeable increase in both voltage and current, delivering the highest power output among all tested configurations.
These tests illustrate how combining series and parallel connections allows for scalable performance tuning, essential for powering low-energy systems reliably.

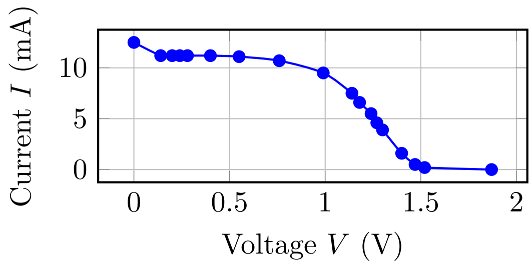

(a) I-V curve

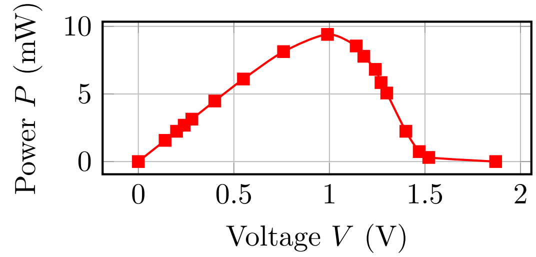

(b) P-V curve

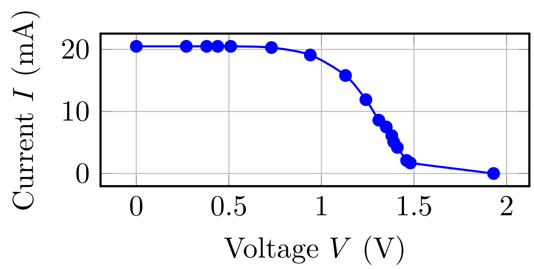

(c) 2 Parallel I-V curve

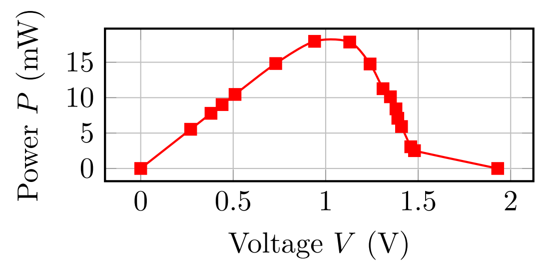

(d) 2 Parallel P-V curve

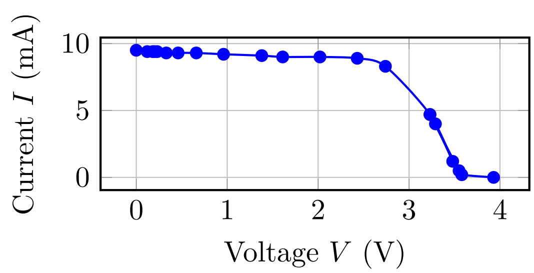

(e) 2 Serie I-V curve

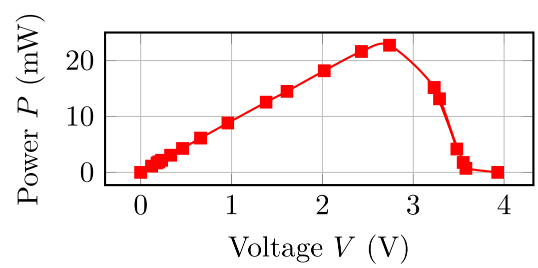

(f) 2 Serie P-V curve

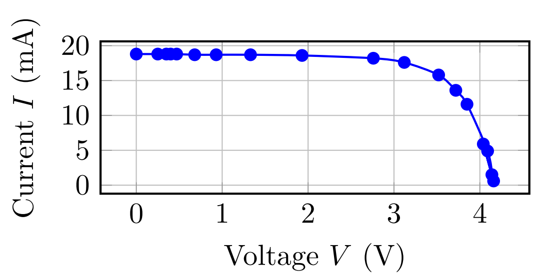

(g) 2X2 config. I-V curve

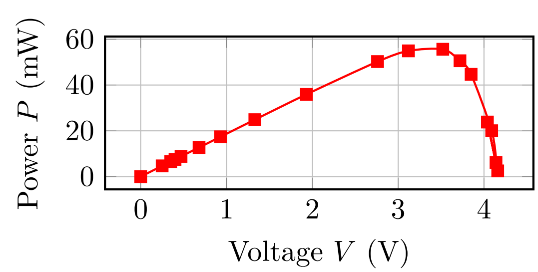

(h) 2X2 config. P-V curve

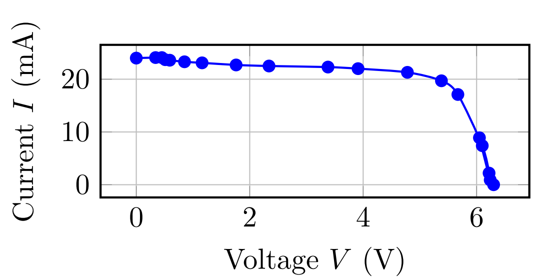

(i) 3X3 config. I-V curve

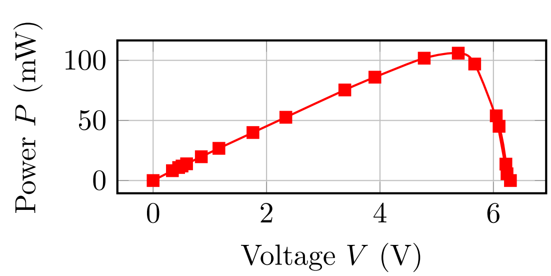

(j) 3X3 config. P-V curve

Figure 3.2: Comparison of the 50x50 mm solar cells

Observations and Discussion

While the figures illustrate the general trends of current and voltage scaling, additional tests were conducted to assess the impact of partial shading—a crucial real-world factor. In these tests, a single cell within both series and parallel configurations was partially shaded.

The results showed that in series configurations, shading one cell drastically reduced the total current, due to the fact that current through a series circuit is limited by the lowest-performing (least illuminated) cell. In contrast, parallel configurations were more robust under the same shading conditions. Although total power output decreased slightly, the current remained significantly higher than in the shaded series case.

These findings emphasize the importance of configuration choice in environments where uniform lighting cannot be guaranteed. For autonomous RA-MIMO repeaters, where consistent power delivery is critical, parallel or hybrid configurations may offer better resilience and efficiency.

3.4 Summary

A comparison of these technologies is summarized below:

Feature	CIGS (Flexible)	Poly/Mono Crystalline (Toy-grade)
Efficiency	11.7 - 16.5%	15 - 18%
Weight	Very light	Moderate
Flexibility	High	None
Shadow tolerance	Limited (in commercial configurations)	Good (in parallel)
Cost	High	Low
Tested in this project	No	Yes

Table 3.1: Solar panel comparison

The solar power supply options are investigated in this chapter. Two types of solar panels are considered: CIGS (flexible) panels and poly/monocrystalline panels (rigid). While CIGS panels offer flexibility and aesthetic integration, they are expensive and less effective under partial shading, due to their connections mostly done in series. The study favored crystalline panels due to their lower cost and better shadow tolerance, especially when configured in parallel. Practical tests and I-V/P-V curve measurements were conducted to validate their performance. Ultimately, polycrystalline cells were selected for further system design considerations.

Chapter 4

Feasible Deployment Areas

To ensure the repeater can operate autonomously year-round using solar energy, it is essential to understand the relationship between power consumption, available solar irradiance, and required panel surface area. This chapter outlines the calculations used and evaluates how feasible deployment is across different European locations.

4.1 Mathematical background

The following steps were used to determine the required solar panel size:

1. **Daily energy demand**
   The daily energy demand E_{demand} can be calculated as:

$$E_{demand} = P_{avg} \cdot t \tag{4.1}$$

   Where $P_{avg} = 6.5W$ (average repeater power) is, and t the operation time.

$$E_{demand} = 156\ Wh/day \tag{4.2}$$

   This is as $t = 24h$

2. **Available Solar Energy**
   Based on weather data [32], the average daily solar energy in winter and summer was taken for multiple cities.

3. **Panel Area Requirement**
   The idea is to make it in the form of a cylinder. But to take into account the inefficiency of this form, a 2/3 efficiency correction factor is included. This was something that was suggested by Professor Uwe Zimmermann.

$$A_{panel} = \frac{E_{demand}}{I_{solar} \cdot \eta \cdot \frac{2}{3}} \tag{4.3}$$

Where:

- I_{solar} : is the average daily sun energy
- η : is the efficiency of solar panel

4.1.1 Height Estimation

To get a better understanding of how big the solar panels need to be, some calculations were done to show how high the cylinder would be. The height is determined using basic formulas for cylinders and taking into account that the cylinder would only be exposed for half of it.

$$h = \frac{A_{panel}}{\pi \cdot r} = \frac{A_{panel}}{\frac{\pi \cdot d}{2}} \tag{4.4}$$

Where:

- r : radius of cylinder
- d : diameter of cylinder

4.2 CIGS solar panel

Initial calculations were made based on flexible CIGS panels due to their ease of installation on curved surfaces. With efficiencies ranging between 11.7% [23] and 16.5% [24], these panels offer a promising solution in theory. In Table 4.1 and Table 4.2 you can find the results for the size based on an efficiency of 14.1% and including the $\frac{2}{3}$ inefficiency factor.

City	**Average Daily Solar Energy Winter (Wh/day)**	**24h (m²)**	**18h (m²)**	**12h (m²)**	**6h (m²)**	**1h (m²)**
Stockholm	200	8.30	6.22	4.15	2.07	0.35
Lund	400	4.15	3.11	2.07	1.04	0.17
Berlin	600	2.77	2.07	1.38	0.69	0.12
Ghent	600	2.77	2.07	1.38	0.69	0.12
Prague	900	1.84	1.38	0.92	0.46	0.08
Paris	800	2.07	1.56	1.04	0.52	0.09
Vienna	1000	1.66	1.24	0.83	0.41	0.07
Bern	1200	1.38	1.04	0.69	0.35	0.06
Zagreb	1200	1.38	1.04	0.69	0.35	0.06
Rome	1700	0.98	0.73	0.49	0.24	0.04
Madrid	2000	0.83	0.62	0.41	0.21	0.03
Athens	2100	0.79	0.59	0.40	0.20	0.03

Table 4.1: Size CIGS panels Winter

City	**Average Daily Solar Energy Summer (Wh/day)**	**24h (m²)**	**18h (m²)**	**12h (m²)**	**6h (m²)**	**1h (m²)**
Stockholm	6200	0.27	0.20	0.13	0.07	0.01
Lund	6400	0.26	0.19	0.13	0.06	0.01
Berlin	6400	0.26	0.19	0.13	0.06	0.01
Ghent	6400	0.26	0.19	0.13	0.06	0.01
Prague	6500	0.26	0.19	0.13	0.06	0.01
Paris	6600	0.25	0.19	0.13	0.06	0.01
Vienna	6700	0.25	0.19	0.12	0.06	0.01
Bern	6900	0.24	0.18	0.12	0.06	0.06
Zagreb	6900	0.24	0.18	0.12	0.06	0.01
Rome	7700	0.22	0.16	0.11	0.05	0.01
Madrid	8300	0.20	0.15	0.10	0.05	0.01
Athens	8100	0.20	0.15	0.10	0.05	0.01

Table 4.2: Size CIGS panels Summer

In Table 4.3 you can find different heights with different diameters. The operation duration is always 24 hours. For different operation durations, the height can be scaled proportionally by the duty cycle.

City	**Height (m)** $d = 16cm$ **Winter**	**Height (m)** $d = 32cm$ **Winter**	**Height (m)** $d = 64cm$ **Winter**	**Height (m)** $d = 16cm$ **Summer**	**Height (m)** $d = 32cm$ **Summer**	**Height (m)** $d = 64cm$ **Summer**
Stockholm	33.02	16.51	8.25	1.07	0.53	0.27
Lund	16.51	8.25	4.13	1.03	0.52	0.26
Berlin	11.01	5.50	2.75	1.03	0.52	0.26
Ghent	11.01	5.50	2.75	1.03	0.52	0.26
Prague	7.34	3.67	1.83	1.02	0.51	0.25
Paris	8.25	4.13	2.06	1.00	0.50	0.25
Vienna	6.60	3.30	1.65	0.99	0.49	0.25
Bern	5.50	2.75	1.38	0.96	0.48	0.24
Zagreb	5.50	2.75	1.38	0.96	0.48	0.24
Rome	3.88	1.94	0.97	0.86	0.43	0.21
Madrid	3.30	1.65	0.83	0.80	0.40	0.20
Athens	3.14	1.57	0.79	0.82	0.41	0.20

Table 4.3: Heights CIGS panels

The calculated heights demonstrate that for winter operation in northern cities such as Stockholm and Lund, CIGS panels would require installation heights exceeding 30 meters on small-diameter poles (16 cm), which is impractical for most urban environments. In contrast, cities in southern Europe, like Athens and Madrid, show significantly lower height requirements—below 4 meters—making them more suitable for year-round, fully solar-powered deployment using CIGS technology.

4.3 Crystalline solar panel

As the project evolved, expert feedback shifted the focus toward small polycrystalline modules. These cells, arranged in parallel, provided better resilience to partial shading and easier customization. Professor Uwe Zimmermann provided some different kinds of solar cells. The average efficiency of those is 14.97% [25–30]. In Table 4.4 and Table 4.5 you can find the different areas needed in different cities in Europe for winter and summer.

City	**Average Daily Solar Energy Winter (Wh/day)**	**24h (m^2)**	**18h (m^2)**	**12h (m^2)**	**6h (m^2)**	**1h (m^2)**
Stockholm	200	7.82	5.86	3.91	1.95	0.33
Lund	400	3.91	2.93	1.95	0.98	0.16
Berlin	600	2.61	1.95	1.30	0.65	0.11
Ghent	600	2.61	1.95	1.30	0.65	0.11
Prague	900	1.74	1.30	0.87	0.43	0.07
Paris	800	1.95	1.47	0.98	0.49	0.08
Vienna	1000	1.56	1.17	0.78	0.39	0.07
Bern	1200	1.30	0.98	0.65	0.33	0.05
Zagreb	1200	1.30	0.98	0.65	0.33	0.05
Rome	1700	0.92	0.69	0.46	0.23	0.04
Madrid	2000	0.78	0.59	0.39	0.20	0.03
Athens	2100	0.74	0.56	0.37	0.19	0.03

Table 4.4: Size Crystalline panels Winter

City	**Average Daily Solar Energy Summer (Wh/day)**	**24h (m^2)**	**18h (m^2)**	**12h (m^2)**	**6h (m^2)**	**1h (m^2)**
Stockholm	6200	0.25	0.19	0.13	0.06	0.01
Lund	6400	0.24	0.18	0.12	0.06	0.01
Berlin	6400	0.24	0.18	0.12	0.06	0.01
Ghent	6400	0.24	0.18	0.12	0.06	0.01
Prague	6500	0.24	0.18	0.12	0.06	0.01
Paris	6600	0.24	0.18	0.12	0.06	0.01
Vienna	6700	0.23	0.18	0.12	0.06	0.01
Bern	6900	0.23	0.17	0.11	0.06	0.06
Zagreb	6900	0.23	0.17	0.11	0.06	0.01
Rome	7700	0.20	0.15	0.10	0.05	0.01
Madrid	8300	0.19	0.14	0.09	0.05	0.01
Athens	8100	0.19	0.14	0.10	0.05	0.01

Table 4.5: Size Crystalline panels Summer

In Table 4.6 you can find different heights with different diameters. The operation duration is always 24 hours. For different operation durations, the height can be scaled proportionally by the duty cycle.

City	Height (m) $d = 16cm$ Winter	Height (m) $d = 32cm$ Winter	Height (m) $d = 64cm$ Winter	Height (m) $d = 16cm$ Summer	Height (m) $d = 32cm$ Summer	Height (m) $d = 64cm$ Summer
Stockholm	31.11	15.55	7.78	1.00	0.50	0.25
Lund	15.55	7.78	3.89	0.97	0.49	0.24
Berlin	10.37	5.18	2.59	0.97	0.49	0.24
Ghent	10.37	5.18	2.59	0.97	0.49	0.24
Prague	6.91	3.46	1.73	0.96	0.48	0.24
Paris	7.78	3.89	1.49	0.94	0.47	0.24
Vienna	6.22	3.11	1.56	0.93	0.46	0.23
Bern	5.18	2.59	1.30	0.90	0.45	0.23
Zagreb	5.18	2.59	1.30	0.90	0.45	0.23
Rome	3.66	1.83	0.91	0.81	0.40	0.20
Madrid	3.11	1.56	0.78	0.75	0.37	0.19
Athens	2.69	1.48	0.74	0.77	0.38	0.19

Table 4.6: Heights Crystalline panels

The height requirements for crystalline solar panels follow a similar pattern to those of CIGS but are slightly more favorable due to higher panel efficiency. In southern regions like Rome and Athens, heights remain well under 4 meters, even on narrow poles. However, in northern locations such as Stockholm and Berlin, winter operation would still require pole-mounted panel heights exceeding 30 meters, reinforcing the need for hybrid power or reduced-duty operation in these areas.

4.4 Summary

This chapter analyzes the feasibility of solar-powered repeater operation across various European cities by estimating the required panel area based on seasonal solar irradiance data. It uses mathematical models to calculate panel surface area and height for cylindrical installations. Results show that full solar autonomy is achievable in southern European cities like Rome and Athens year-round. However, in northern cities such as Stockholm or Berlin, the required panel size becomes impractical in winter, suggesting that a hybrid power solution (solar + grid) may be necessary in those regions.

Chapter 5

Charge controller

A charge controller is a critical component in solar-powered systems, acting as the interface between the photovoltaic (PV) source and the energy storage (battery). Its main function is to regulate the charging process, ensuring safe and efficient energy transfer while protecting the battery from overcharging, over-discharging, and thermal stress. This chapter presents an overview of the types of charge controllers, compares multiple Maximum Power Point Tracking (MPPT) algorithms, and concludes with the final design implemented using the BQ25756 IC [2], chosen for its suitability in this low-power, solar-powered 5G repeater system. In solar energy systems, energy harvesting efficiency is directly influenced by how well the controller can track the panel's maximum power point under dynamic conditions. Factors such as solar irradiance, temperature, and shading cause the I-V curve of a solar panel to change continuously. A charge controller must therefore adapt in real time to extract the maximum possible energy without damaging the battery. To support the development of this section, several relevant works were reviewed for foundational insights into charge controller operation and MPPT strategies [33–35]. Additional literature was consulted for a broader perspective, though not directly cited due to substantial overlap in content.

5.1 Types of Charge Controllers

Two primary classes of charge controllers are used in practice [33, 34]:

- **Pulse Width Modulation(PWM) Controllers**
  PWM controllers regulate current by switching the connection to the battery on and off. While inexpensive and suitable for small systems, PWM controllers are less efficient under changing environmental conditions and do not always operate at the panel's maximum power point.

- **Maximum Power Point Tracking (MPPT) Controllers**
  MPPT controllers dynamically adjust the load seen by the solar panel to ensure operation at the point of maximum power output. They typically use DC-DC converters (buck, boost, or buck-boost) to match the panel voltage to the optimal charging conditions of the battery.

Given the efficiency demands and variable sunlight conditions of this project, an MPPT-based controller was clearly more appropriate.

5.2 MPPT Algorithms

Several MPPT algorithms exist, each with trade-offs between complexity, tracking speed, and robustness. A comparative review of the most common techniques was performed during the research phase [35].

5.2.1 Perturb and Observe (P&O)

The Perturb & Observe (P&O) algorithm is one of the most used algorithms for Maximum Power Point Tracking (MPPT) in photovoltaic (PV) systems. This is due to its simplicity and ease of implementation. It works by perturbing (adjusting) the voltage or duty cycle of the system and observing the resulting change in power. If the power increases, the perturbation continues in the same direction. If the power decreases, the direction of perturbation is reversed.
This iterative process helps track the Maximum Power Point (MPP). However, P&O suffers from oscillations around a local MPP, leading to power losses and struggles in rapidly changing environmental conditions. Despite these drawbacks, its low cost and minimal computation requirements make it a popular choice for basic MPPT applications.

- **Advantages:** Simple, low computational load
- **Disadvantages:** Oscillates around local MPP, performs poorly under rapidly changing irradiance

5.2.2 Incremental Conductance (INC)

The Incremental Conductance (INC) algorithm improves upon P&O by using the derivative of the power-voltage curve to determine the MPP more accurately. It calculates the incremental conductance ($\frac{dI}{dV}$) and compares it to the instantaneous conductance ($\frac{I}{V}$).
$\frac{dI}{dV} = -\frac{I}{V}$ at the MPP.
$\frac{dI}{dV} > -\frac{I}{V}$ at the left of the MPP, increase voltage.
$\frac{dI}{dV} < -\frac{I}{V}$ at the right of the MPP, decrease voltage.
This approach reduces oscillations and improves tracking efficiency, especially under varying irradiance. However, INC is computationally more demanding than P&O, requiring more complex calculations. It offers better accuracy and faster response in dynamic conditions, making it a preferred choice for more advanced MPPT applications.

- **Advantages:** More accurate, better under changing light
- **Disadvantages:** More complex, requires precise current and voltage measurements

5.2.3 Artificial Neural Network (ANN)

Artificial Neural Networks (ANN) are increasingly being used in MPPT controllers to optimize the efficiency of solar systems. Unlike traditional MPPT methods such as P&O or INC, ANN-based MPPT algorithms leverage machine learning to predict the MPP dynamically.
ANNs are trained using historical data, including irradiance, temperature, and voltage-current characteristics of the PV panel. Once trained, the network can quickly adapt to varying environmental conditions and provide fast, accurate MPP tracking with minimal oscillations. This results

in higher efficiency, reduced energy losses, and improved system stability compared to conventional methods.
The implementation of ANN in MPPT controllers requires a well-structured neural network, typically with an input layer (sensor data), one or more hidden layers (processing units) and an output layer (optimal duty cycle for the DC-DC converter).

- **Advantages:** Fast, accurate, resilient to partial shading
- **Disadvantages:** Requires training data, high computation demand

5.2.4 Particle Swarm Optimization (PSO)

Particle Swarm Optimization (PSO) is a bio-inspired optimization technique that has been effectively applied to Maximum Power Point Tracking (MPPT) in photovoltaic (PV) systems. PSO is based on the social behavior of swarms, such as birds or fish, and is used to find the optimal operating point of a PV system under varying environmental conditions.
In a PSO-based MPPT controller, a set of particles (potential solutions) explores the search space, representing different duty cycles of the DC-DC converter. Each particle adjusts its position based on its own best-known solution and the best solution found by the swarm. Through iterative updates, the algorithm converges to the global (MPP) with high accuracy and reduced steady-state oscillations compared to traditional methods like P&O.
PSO offers advantages such as fast convergence, robustness to partial shading conditions, and the ability to escape local maxima. However, its performance depends on proper parameter tuning, including swarm size, inertia weight, and acceleration coefficients. With advancements in microcontrollers and real-time processing, PSO has become a viable and efficient solution for improving MPPT efficiency in solar energy systems.

- **Advantages:** Avoids local maxima, robust in complex conditions
- **Disadvantages:** Slower startup, computationally heavier than P&O/INC

5.3 BQ25756-based MPPT Controller

5.3.1 Prototype implementation and motivation

For the first prototype of the solar charge controller, the Texas Instruments BQ25756 [2] was selected as the core component. Another component that was considered was the LT8490 by Analog Devices [36]. However, the BQ25765 was chosen because it offers inter-integrated circuit (I^2C) communication, which proved useful for debugging and configuring various safety features. The BQ25756 integrated buck-boost battery charge controller includes built-in MPPT functionality, making it ideal for low-power, solar-powered applications such as our 5G repeater.
The primary motivation for choosing this component lies in its flexibility, high efficiency, and intelligent MPPT tracking capabilities. Given that the input voltage from solar panels can vary significantly depending on weather conditions and panel configuration, it was critical to select a charge controller that could adapt to a wide range of input voltages.

5.3.2 MPPT with P&O and Full I-V Sweep

Unlike basic controllers that use a static P&O approach and risk getting stuck in local maxima—especially under partial shading, the BQ25756 enhances this algorithm by periodically performing a full sweep of the I-V curve. This ensures that the controller always seeks the global maximum power point.
This behavior is particularly advantageous for autonomous systems like ours, where maximizing the energy yield directly affects the system's runtime.

5.3.3 Output and Input Configuration

In the prototype, the input range is kept as wide as the BQ25756 allows (4.2 - 70 V), enabling compatibility with different types and configurations of solar panels. The output can also vary from batteries that are just 1 cell to 14 cells in series. In this prototype, it is designed to have an output of 25.2V, but with just changing one resistor, this can be changed. This is also a flexibility that is very useful in this project.

5.3.4 Safety Features

The BQ25756 MPPT charge controller incorporates a comprehensive set of safety features designed to protect both the system and battery during solar-powered operation.

- **Input overvoltage and undervoltage protection:** The controller continuously monitors the input voltage and will suspend charging if the input falls outside the programmed safe range, preventing damage from excessive or insufficient supply voltages.
- **Battery overvoltage and overcurrent protection:** It provides strict monitoring of the battery voltage and current, immediately terminating charging if thresholds are exceeded, thereby safeguarding battery health and extending lifespan.
- **Battery short-circuit protection:** In the event of a battery short, the device promptly detects the condition and halts charging to avoid catastrophic failure.
- **Charging safety timer:** An integrated safety timer ensures that charging cannot continue indefinitely, protecting against prolonged faults conditions or failed charge termination.
- **Thermal Shutdown:** Using thermistor input, the BQ25756 suspends charging if the battery temperatures falls outside the user-defined safe window, thus ensuring safe operation across a range of environmental conditions.
- **Status monitoring and Fault reporting:** Dedicated status pins and I^2C reporting allow real-time indictaion and monitoring of system faults, including power status and detailed charge operation/fault states.

These integrated protection mechanisms make the BQ25756 particularly well-suited for autonomous and remote solar charging systems, where hardware-level safety is essential for reliability and long-term operation.

5.3.5 Advantages over Alternatives

Alternative designs such as PWM controllers or discrete MPPT implementations with microcontrollers were considered but rejected for the following reasons:

- PWM controllers are inefficient under variable irradiance and do not track the true MPP.
- Custom MPPT solutions require significant development time and often lack full-sweep functionality.
- Other MPPT ICs may be limited to buck or boost only, whereas the BQ25756 supports buck-boost operation—crucial for varying voltage conditions.

The integrated I^2C interface also simplifies monitoring and control, allowing data collection and system diagnostics via a microcontroller in the repeater system.

5.3.6 Block Diagram

Figure 5.1 illustrates the system-level block diagram of the solar-powered charge controller implemented in this project. The figure highlights its interaction with key components: the solar panel, battery, system load, and a microcontroller (ESP32). The ESP32 is used to configure and monitor the BQ25765 charger IC via I^2C communication. It reads various voltage and current registers. Its built-in wireless capabilities make it ideal for remote supervision and future integration into IoT-based monitoring platforms.
The diagram consists of the following key elements:

- **Solar Panel**: Acts as the primary energy source, delivering variable DC power depending on solar irradiance conditions. Its output is connected directly to the input of the BQ25756.
- **BQ25756 MPPT Controller**: This is the core of the power management system. It performs:
  - **MPPT (Maximum Power Point Tracking)** using a hybrid P&O and periodic full I-V sweep algorithm.
  - **Voltage regulation** through a buck-boost converter, adapting the input voltage to the battery charging requirements.
  - **Battery protection**, managing safe charging via overvoltage, current, and thermal protections.
  - **System power routing**, allowing power delivery to both the battery and the system load in parallel.
- **Battery**: Stores harvested energy and provides continuous power to the load, especially during low or no sunlight. The battery is directly charged and managed by the BQ25756.
- **Load**: Represents the actual repeater system or other connected electronics that draw power from the battery (and indirectly from solar input). It receives regulated voltage either from the battery or directly via the controller.
- **ESP32 Microcontroller**: Interfaces with the BQ25756 via I^2C communication. It is responsible for real-time monitoring of voltage, current, and system status. It can also log data, perform diagnostics, or communicate wirelessly with external systems if needed.

This configuration supports **autonomous solar-powered operation** while enabling robust battery management and system diagnostics—making it suitable for remote RA-MIMO repeater deployments.

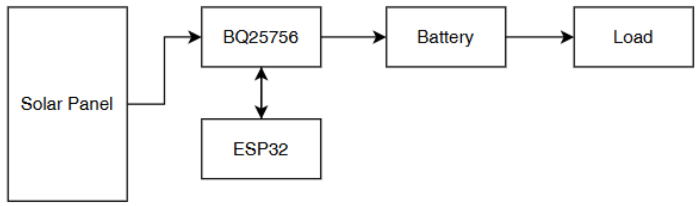

Figure 5.1: Charge Controller block diagram

5.3.7 Schematic

The schematic of the charge controller was designed in KiCad, based on the Texas Instruments BQ25756 datasheet and reference design. The initial design targeted a 4S Li-ion battery, but later testing was also done with a lower-voltage battery. This change only required adjusting a single resistor value, illustrating the flexibility of the IC to support different battery configurations with minimal hardware modifications. To support a wide input voltage range, some elements from the reference schematic were modified or omitted. For example, some hardware-set thresholds were intentionally left out, as these would be configured in software via I^2C during runtime. This decision enabled a cleaner and more adaptable prototype, aligned with future plans for software-managed behavior. The schematic also reflects design choices made for rapid testing and debugging, particularly the integration of an ESP32 for I^2C control and monitoring. Overall, the design prioritizes adaptability and was optimized for quick iteration rather than rigid adherence to the datasheet example.
The schematic can be found in the appendix.

5.3.8 Problems

Because this is a first prototype, there could be some problems with it. A first problem was that it was always stuck in non-charging mode, and there was no gate voltage on the REGN and DRV pin. After some debugging and googling, this was fixed by shorting pins 32 and 33. Figures 5.2, 5.3, 5.4 and 5.5 can show different stages of charging, that yo can see in Figure 5.6, that match the different stages mentioned in the datasheet [2]. As you can see on the line with IBAT_ADC, there is no current flowing. This is still a problem that needs to be fixed. From measurement, the most likely problem would be that there is still something wrong with the output. After some measurements, it could be concluded that the signals from the MOSFETs are good. So there is probably a shortcut in the sense resistor at the output. But due to time limit, this could not be further examined.

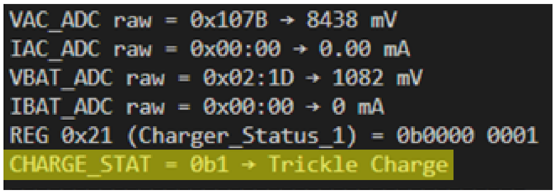

```
VAC_ADC raw = 0x107B → 8438 mV
IAC_ADC raw = 0x00:00 → 0.00 mA
VBAT_ADC raw = 0x02:1D → 1082 mV
IBAT_ADC raw = 0x00:00 → 0 mA
REG 0x21 (Charger_Status_1) = 0b0000 0001
CHARGE_STAT = 0b1 → Trickle Charge
```

Figure 5.2: Trickle Charge

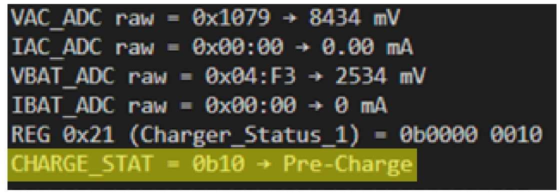

```
VAC_ADC raw = 0x1079 → 8434 mV
IAC_ADC raw = 0x00:00 → 0.00 mA
VBAT_ADC raw = 0x04:F3 → 2534 mV
IBAT_ADC raw = 0x00:00 → 0 mA
REG 0x21 (Charger_Status_1) = 0b0000 0010
CHARGE_STAT = 0b10 → Pre-Charge
```

Figure 5.3: Pre-charge

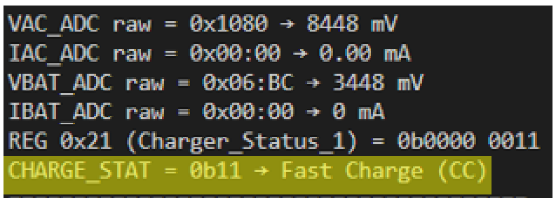

```
VAC_ADC raw = 0x1080 → 8448 mV
IAC_ADC raw = 0x00:00 → 0.00 mA
VBAT_ADC raw = 0x06:BC → 3448 mV
IBAT_ADC raw = 0x00:00 → 0 mA
REG 0x21 (Charger_Status_1) = 0b0000 0011
CHARGE_STAT = 0b11 → Fast Charge (CC)
```

Figure 5.4: Fast Charge

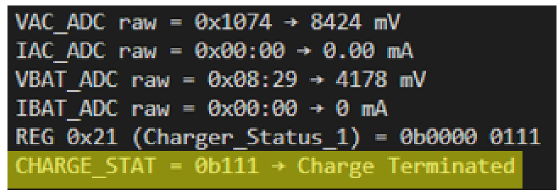

```
VAC_ADC raw = 0x1074 → 8424 mV
IAC_ADC raw = 0x00:00 → 0.00 mA
VBAT_ADC raw = 0x08:29 → 4178 mV
IBAT_ADC raw = 0x00:00 → 0 mA
REG 0x21 (Charger_Status_1) = 0b0000 0111
CHARGE_STAT = 0b111 → Charge Terminated
```

Figure 5.5: Charge Terminated

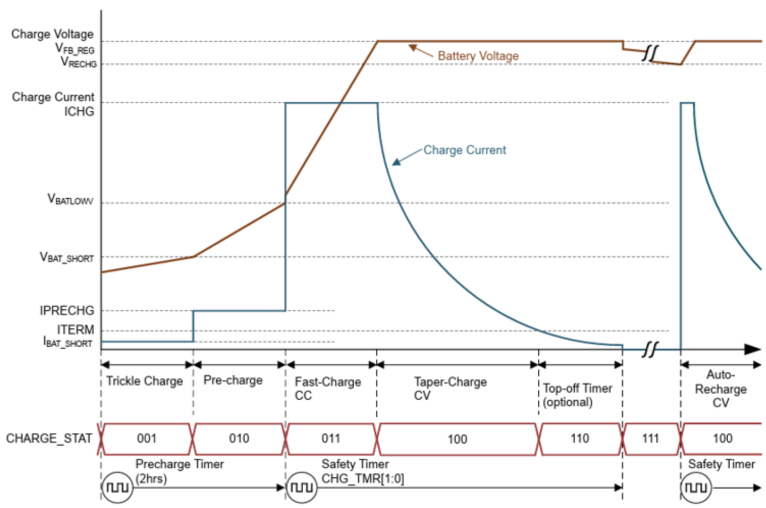

Figure 5.6: Charge stages

5.4 Summary

The focus here is on selecting and configuring an efficient charge controller to manage solar energy harvesting and battery charging. Various MPPT (Maximum Power Point Tracking) algorithms are compared, including Perturb & Observe (P&O), Incremental Conductance (INC), Artificial Neural Networks (ANN), and Particle Swarm Optimization (PSO). The Texas Instruments BQ25756 chip was selected for the prototype due to its integrated MPPT features, wide voltage support, and safety mechanisms. While initial testing encountered some technical issues (e.g., charging stuck), the controller proved suitable for managing power flow in dynamic solar conditions, providing a strong base for future development.

Chapter 6

Conclusions and future work

6.1 Conclusions

This thesis explored the feasibility of developing a sustainable, low-power repeater for Repeater-Assisted MIMO (RA-MIMO) systems, focusing on solar-powered operation for off-grid deployment. The research investigated both system architecture and environmental viability through a component-level energy analysis and evaluation of solar energy availability across Europe.

An analog amplify-and-forward repeater was selected for its simplicity, low latency, and energy efficiency. A detailed breakdown of subsystem power consumption resulted in an estimated average requirement of 6.5 W, guiding the dimensioning of the solar power system.

To power the system sustainably, two types of solar panels were analyzed—flexible CIGS and rigid polycrystalline modules. While CIGS offers mechanical flexibility, polycrystalline cells were ultimately favored for their lower cost, better availability, and superior performance under partial shading. Practical tests confirmed the advantages of using small, parallel-connected panels in real-world conditions.

Solar irradiance data for multiple European cities showed that year-round autonomous operation is achievable in southern locations, such as Athens, Rome, and Madrid. However, northern cities with limited winter sunlight (e.g., Stockholm, Berlin) would require oversized panels or supplementary power sources, making hybrid solar-grid solutions more practical for those regions.

The system's power efficiency is expected to depend heavily on the performance of the MPPT charge controller. The selected BQ25756 controller, with its built-in power tracking and wide voltage range, appears to be a strong candidate for maintaining energy harvesting under variable conditions, although some issues were encountered during early prototyping.

In conclusion, this study suggests that a compact, solar-powered 5G repeater *could* be a technically feasible solution—particularly in regions with moderate to high solar availability and when operating at a reduced duty cycle. While the concept may not yet be universally viable without another supply source, it represents a promising direction for sustainable, scalable wireless infrastructure, especially in rural or temporary deployment scenarios.

6.2 Future Work

Several opportunities for continued research and development emerged during the course of this project:

- Full 5G Repeater Implementation: The next logical step is to move beyond the architectural and power feasibility analysis and begin work on an actual 5G-compatible analog repeater prototype. This includes designing the RF front-end, ensuring compliance with 5G frequency bands, and validating the system against key performance metrics.
- MPPT Algorithm Evaluation: The selected solar charge controller is based on a fixed MPPT approach. However, there are numerous MPPT algorithms (Perturb and Observe, Incremental Conductance, etc.) that vary in performance depending on lighting conditions and load profiles. Future work should involve testing and benchmarking different MPPT strategies to determine which algorithm provides the highest energy yield under partial shading and intermittent loads. This could lead to improved or custom-designed MPPT controller hardware tailored for low-power wireless systems.
- Advanced Power Management Strategies: Incorporating intelligent sleep modes, adaptive duty cycles, and context-aware energy scheduling may allow for more efficient use of harvested energy. Such features could further reduce power consumption and extend operational lifetime, especially in autonomous rural deployments.

In summary, while a fully autonomous, solar-powered 5G repeater is not universally feasible in all conditions, this thesis has shown that under the right constraints and with smart design choices, a sustainable repeater system is within reach. Future advancements in low-power electronics, adaptive power management, and solar charging technologies could further expand the applicability of such systems in next-generation wireless networks.

References

[1] S. Willhammar, H. Iimori, J. Vieira, L. Sundström, F. Tufvesson, and E. G. Larsson, "Achieving distributed MIMO performance with repeater-assisted cellular massive MIMO," *IEEE Communications Magazine*, vol. 63, no. 3, pp. 114–119, 2025. doi: 10.1109/MCOM.001.2400332.

[2] Texas Instruments, "BQ25756: Stand-alone/I²C-Controlled 1- to 14-Cell Bidirectional Buck-Boost Battery Charge Controller with MPPT," product page. [Online]. Available: https://www.ti.com/product/BQ25756/ (accessed April, 2025).

[3] S. Allen, "What will the role of signal repeaters and boosters be in 5G networks?" *RCR Wireless News*, Oct. 12, 2020. [Online]. Available: `https://www.rcrwireless.com/20201012/5g/what-will-the-role-of-signal-repeaters-and-boosters-be-in-5g-networks`

[4] Airgain, "Lighthouse Micro Smart Repeater," *Airgain*. [Online]. Available: `https://web.archive.org/web/20250123160446/https://www.airgain.com/products/lighthouse-micro-smart-repeater/` (accessed Mar. 2025).

[5] T. Li, M. H. Mazaheri, and O. Abari, "Enabling On-Demand Low-Power mmWave Repeaters via Passive Beamforming," in *Proc. ACM MobiCom*, Oct. 2024, pp. 618–632.

[6] A. Schumacher, R. Merz, and A. Burg, "Increasing Cellular Network Energy Efficiency for Railway Corridors," in *Proc. Design, Automation & Test in Europe Conf. & Exhibition (DATE)*, 2022, pp. 1103–1106, doi: 10.23919/DATE54114.2022.9774757.

[7] Z. Niu and H. Xue, "A novel portable repeater for 5G applications," in *Proc. 2024 IEEE Int. Black Sea Conf. Commun. Netw. (BlackSeaCom)*, 2024, pp. 186–191, doi: 10.1109/BlackSeaCom61746.2024.10646245.

[8] Askey, "SCU2060 5G Smart Repeater," Askey. [Online]. Available: https://www.askey.com/products-detail/scu2060/ (accessed Mar. 2025).

[9] WilsonPro, *Pro 70 Plus – 75 Booster* [Online]. Available: https://www.wilsonpro.com/products/pro-70-plus-75-ohm-booster [Accessed: Mar. 2025].

[10] SureCall, "Fusion4Home Max," SureCall. [Online]. Available: https://surecall.com/cell-signal-boosters-for-mid-sized-homes/fusion4home-max/ (accessed Mar. 2025).

[11] Hocell, “5G Cellular Signal Booster (HWSR-Pico Series),” Hocell Information Technologies, Shenzhen, China. [Online]. Available: https://www.hocell.com/productinfo/496501.html (accessed Mar. 2025).

[12] Hocell, “2T2R 5G Cellular Signal Booster,” Hocell Information Technologies, Shenzhen, China. [Online]. Available: https://www.hocell.com/productinfo/698055.html (accessed Mar. 2025).

[13] WilsonPro, “Network 257 Repeater,” WilsonPro. [Online]. Available: https://www.wilsonpro.com/products/network_257 (accessed Mar. 2025).

[14] WilsonPro, *Enterprise 1337R* [Online]. Available: https://www.wilsonpro.com/products/enterprise-1337r [Accessed: Mar. 2025].

[15] Qorvo, Inc., “Qorvo Product Portfolio,” 2025. [Online]. Available: https://www.qorvo.com/products (accessed Mar. 2025).

[16] Analog Devices, Inc., “Analog Devices Product Selector Guide,” 2025. [Online]. Available: https://www.analog.com/en/products.html (accessed Mar. 2025).

[17] Skyworks Solutions, Inc., “Skyworks RF Portfolio,” 2025. [Online]. Available: https://www.skyworksinc.com/en/products (accessed Mar. 2025).

[18] Arctic Semiconductor, “Arctic Semiconductor,” 2025. [Online]. Available: https://arcticsemiconductor.com/ (accessed May 2025).

[19] u-blox AG, “u-blox ,” 2025. [Online]. Available: https://www.u-blox.com/en (accessed May 2025).

[20] Quectel Wireless Solutions, “Quectel,” 2025. [Online]. Available: https://www.quectel.com/ (accessed May 2025).

[21] Cinterion (Thales), “Cinterion,” 2025. [Online]. Available: https://www.telit.com/(accessed May 2025).

[22] MultiTech Systems, Inc., “MultiTech IoT Gateways & Modems,” 2025. [Online]. Available: https://www.multitech.com/brands/multiconnect-conduit (accessed May 2025).

[23] Midsummer, “CIGS Solar Panel Midsummer,” Midsummer. [Online]. Available: https://midsummer.se/en/midsummer-bold/ (accessed Mar. 2025).

[24] MiaSolé, “CIGS Solar Panel MiaSolé,” MiaSolé. [Online]. Available: https://miasole.com/products/ (accessed Mar. 2025).

[25] Velleman, “SOL4N Polycrystalline Solar Cell,” Amazon.se. [Online]. Available: https://www.amazon.se/Velleman-SOL4N-polykristallin-solcell-flerf%C3%A4rgad/dp/B07BQPX344/ (accessed Apr. 2025).

[26] Unknown brand, “Solpanel Polycrystalline Silicon Scientific Project,” Amazon.se. [Online]. Available: https://www.amazon.se/Solpanel-Polykristallin-Silicon-Vetenskapliga-Projekt/dp/B0DD48NW7K/(accessed Apr. 2025).

[27] AliExpress, “Mini Solar Panel 5 V 1 W DIY Solar Cell Module Charger,” 2025. [Online]. Available: https://www.aliexpress.com/item/1005004580265551.html (accessed Apr. 2025).

[28] AliExpress, “Solar Panel 6 V 1.5 W Polycrystalline Solar Cell Module,” 2025. [Online]. Available: https://www.aliexpress.com/item/32893735749.html (accessed Apr. 2025).

[29] AliExpress, “USB Solar Panel 6 V 3 W with USB Output Module Charger,” 2025. [Online]. Available: https://www.aliexpress.com/item/1005008195178742.html (accessed Apr. 2025).

[30] AliExpress, “6 V 2 W Mini Solar Panel Epoxy Polycrystalline Silicon,” 2025. [Online]. Available: https://www.aliexpress.com/item/4000282864109.html (accessed Apr. 2025).

[31] C. Honsberg and S. Bowden, "Effect of Temperature," *PVEducation*, https://www.pveducation.org/pvcdrom/solar-cell-operation/effect-of-temperature (accessed July, 2025).

[32] WeatherSpark, “Beautiful Weather Graphs and Data,” [Online]. Available: https://weatherspark.com/ (accessed May 2025).

[33] C. A. Osaretin and F. O. Edeko, “Design and implementation of a solar charge controller with variable output,” *Electrical and Electronic Engineering*, vol. 12, no. 2, pp. 40–50, 2015.

[34] T. Majaw, R. Deka, S. Roy, and B. Goswami, “Solar charge controllers using MPPT and PWM: A review,” *ADBU J. Electr. Electron. Eng. (AJEEE)*, vol. 2, no. 1, 2018.

[35] S. Motahhir, A. El Hammoumi, and A. El Ghzizal, “The most used MPPT algorithms: Review and the suitable low-cost embedded board for each algorithm,” *J. Clean. Prod.*, vol. 246, p. 118983, Jan. 2020. doi: 10.1016/j.jclepro.2019.118983.

[36] Analog Devices, *LT8490 - Buck-Boost Battery Charging Controller with MPPT*, [Online]. Available: https://www.analog.com/en/products/lt8490.html [Accessed: April 2025].

Appendix A
Schematic

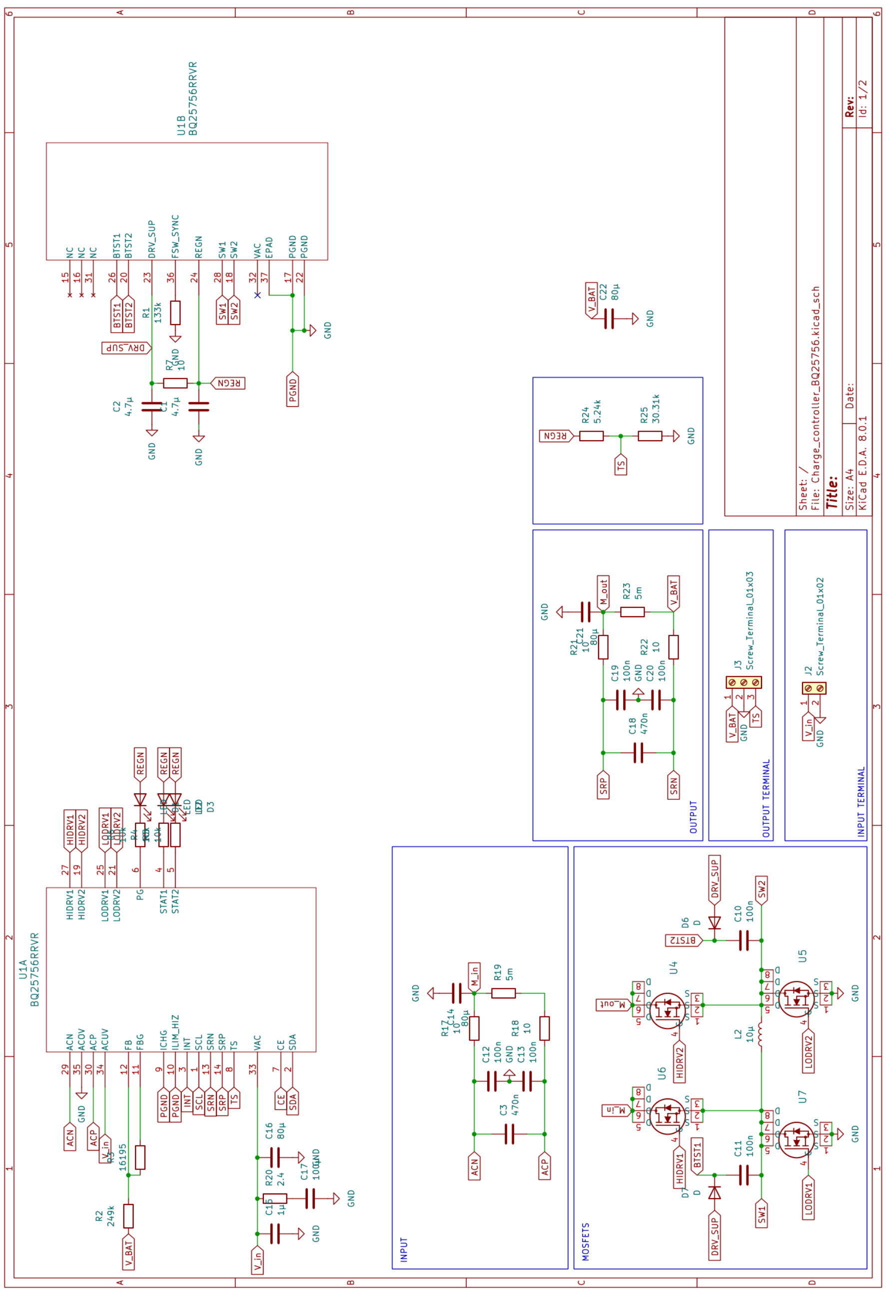

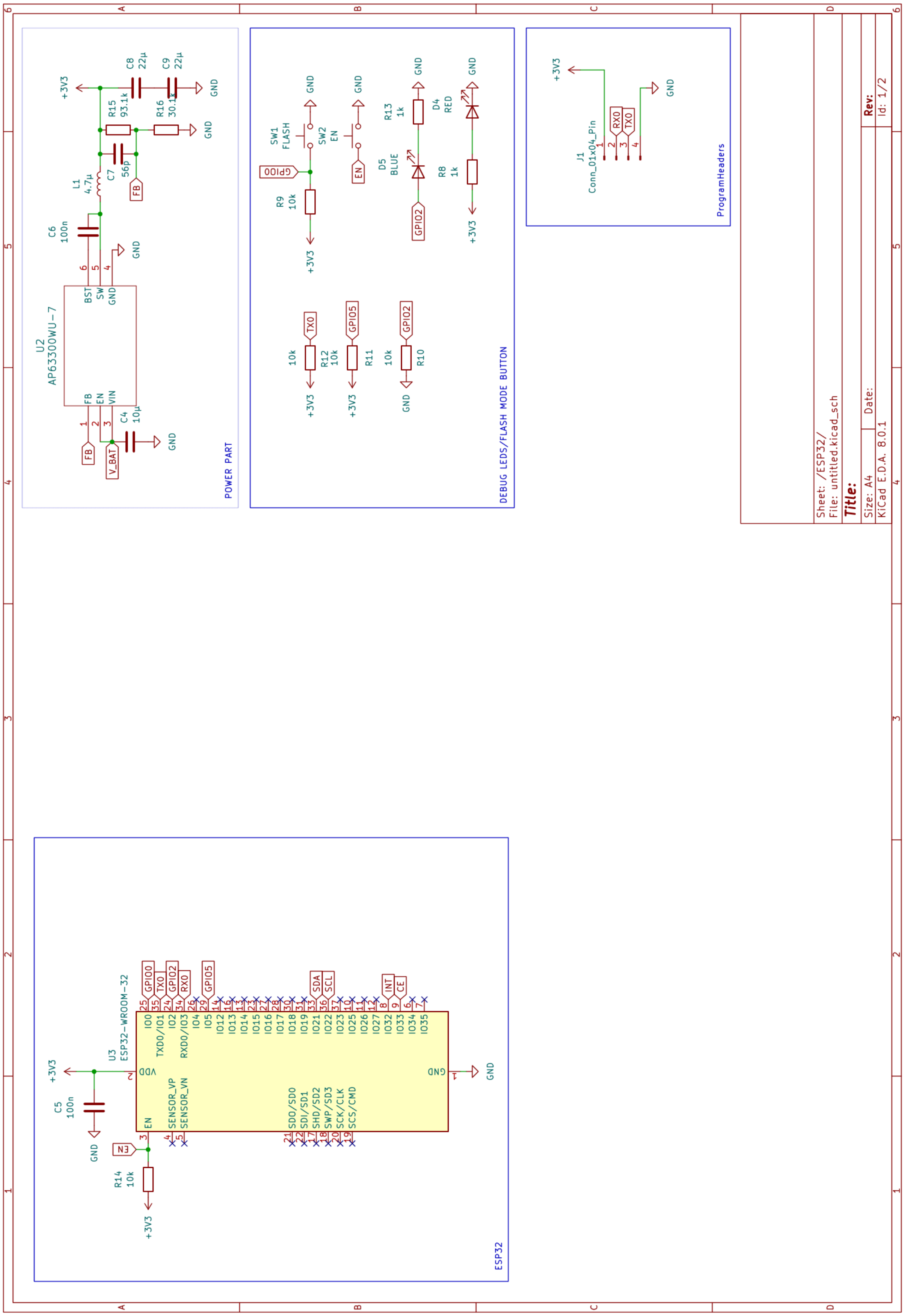
POWER PART
U2
AP63300WU-7
C4 10µ
C6 100n
L1 4.7µ
C7 56p
R15 93.1k
R16 30.1k
C8 22µ
C9 22µ
V_BAT
DEBUG LEDS/FLASH MODE BUTTON
SW1 FLASH
SW2 EN
D5 BLUE
D4 RED
R13 1k
R8 1k
R9 10k
R10 10k
R11 10k
R12 10k
ProgramHeaders
J1
Conn_01x04_Pin
ESP32
U3
ESP32-WROOM-32
R14 10k
C5 100n
Sheet: /ESP32/
File: untitled.kicad_sch
Title:
Size: A4
Date:
KiCad E.D.A. 8.0.1
Rev:
Id: 1/2